Analyst

Accepted Manuscript

ROYAL SOCIETY OF CHEMISTRY

www.rsc.org/analyst

3D elemental sensitive imaging by full field XFCT

Biao Deng*, Guohao Du, Guangzhao Zhou, Yudan Wang, Yuqi Ren, Rongchang Chen, Pengfei Sun, Honglan Xie, Tiqiao Xiao**

Shanghai Institute of Applied Physics, Chinese Academy of Sciences
Zhangheng Road 239, 201204 Shanghai,China
*E-mail:dengbiao@sinap.ac.cn; **E-mail:tqxiao@sinap.ac.cn

Abstract:

X-ray fluorescence computed tomography(XFCT) is a stimulated emission tomography modality that maps the three-dimensional(3D) distribution of elements. Generally, XFCT is done by scanning a pencil-beam across the sample. This paper presents a feasibility study of full field XFCT(FF- XFCT) for 3D elemental imaging. The FF-XFCT consists of a pinhole collimator and X-ray imaging detector with no energy resolution. A prototype imaging system was set up at the Shanghai Synchrotron Radiation Facility(SSRF) for imaging the phantom. The first FF-XFCT experimental results are presented. The cadmium(Cd) and iodine(I) distributions were reconstructed. The results demonstrate FF-XFCT is fit for 3D elemental imaging and the sensitivity of FF-XFCT is higher than conventional CT system.

Key words: FF-XFCT, Elemental imaging , Synchrotron radiation

Introduction

X-ray fluorescence computed tomography(XFCT), combining X-ray fluorescence microanalysis with tomographic techniques, can obtain the element distribution on an arbitrary virtual section through the sample without the need for destructive sample preparation. XFCT has been applied in the fields of botany, biomedical, medicine, material, mineralogy [1-7] and so on. In typical XFCT studies, the sample is scanned line by line with a pencil beam of synchrotron X-rays, which takes an enormous amount of acquisition time to acquire a 3D tomographic image. In order to overcome this difficulty, some new data acquisition modes was proposed to accelerate the image acquisition. Geng Fua et al. [8] have proposed a novel imaging geometries for XFCT studies with a position- and energy-sensitive detector collimated by one or more pinholes. However, the high performance position- and energy-sensitive detectors is ongoing studies [9-10] and there is no off-the-shelf product. So

such a detector is every expensive. N. Sunaguchi, et al [11] propose a XFCT using a pinhole methodology which utilizes an X-ray CCD (charge coupled device) camera with no energy resolution. But it just fit for one element imaging in the sample.

In this paper, we propose a feasibility study to perform 3D elemental imaging for multiple elements of interest within a single sample using full field X-ray fluorescence computed tomography(FF- XFCT). The FF-XFCT consists of a pinhole collimator and X-ray imaging detector with no energy resolution. A prototype imaging system was set up at the Shanghai Synchrotron Radiation Facility(SSRF) for imaging the phantom. The capability of the proposed method is confirmed by an experiment for imaging phantoms which contain solutions of two elements.

Methods and materials

FF-XFCT is based on the same geometric principle as the pinhole SPECT [12]. Fig.1 is the sketch of FF-XFCT with pinhole collimator. Instead of using a pencil-beam of synchrotron X-rays, the object is illuminated with a whole-volume incident beam, X-ray fluorescence photons are collected by an X-ray imaging detector using a pinhole collimator with no energy resolution. Since photons travel in straight lines, an inverted image of the illuminated field of view is produced when they pass through a pinhole. The size of the projected image depends on the relative distance between object and pinhole versus pinhole and the surface where the image is projected. When meet the appropriate imaging geometry, magnification of the projected image can be obtained.

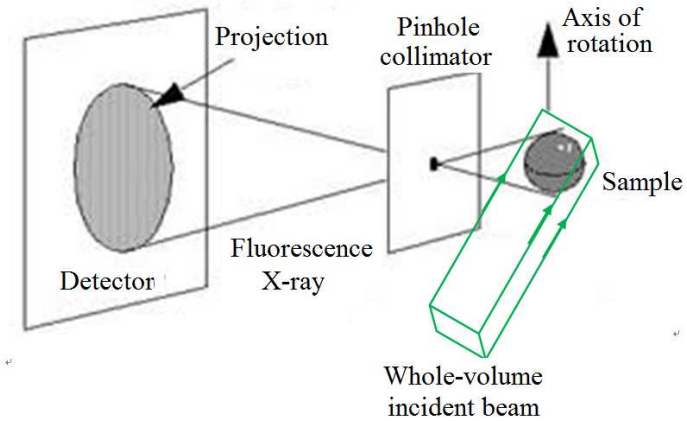

Fig. 1. The sketch of FF-XFCT with pinhole collimator

A prototype FF-XFCT system using X-ray imaging detector with no energy resolution was constructed at the beamline BL13W1 of Shanghai Synchrotron Radiation Facility(SSRF). Fig.2 presents the layout of the FF-XFCT system at SSRF. The white beam from 2 Tesla wiggler is monochromatized by a double crystal liquid nitrogen-cooled monochromator. The fundamental radiation covers the energy range from 8.0 to 72.5 keV. **T**he maximal unfocused monochromatic beam size at the sample is 45mm(h)×5mm(v) and it is very suitable for full field XFCT imaging. A high-precision sample stage is used for positioning and/or rotating the sample. The collimator is a 2 mm-thick lead plate with a pinhole of 500μm in diameter. The X-ray CCD (Photonic Science, FDI-VHR) with pinhole are used for detecting the fluorescent photons, which was placed at the 90^0 direction from the incident X-ray beam to minimize scattering photons. Another X-ray CCD camera is used for detecting the transmission x-rays for transmission CT. A silicon drift detector (SDD) is used to verify the presence of different elements in the illuminated area on the sample.

Ordered-subsets expectation maximization algorithm, which is based on statistical theory has been proved to be accurate in stimulated emission tomography (e.g. PET,SPECT) reconstruction and is able to reconstruct with limited angle projection data. XFCT is a stimulated emission tomography modality. Inspired by the image reconstruction in PET and SPECT, OSEM algorithm have been introduced to XFCT[13]. For OSEM reconstruction algorithm in XFCT, the object is divided into an I×I pixel matrix. M angular views and N translations were employed. The elemental distribution to be estimated is defined as C(i,j)(i=1,2,…,I; j=1,2,…,I) and the projection values are denoted as I(m,n)(m=1,2,…,M;n=1,2,…,N), K(i,j,m,n) represents the contribution of pixel (i,j) to projection value of (m,n). S1,S2,…SL. describe the chosen subsets. Cl+1(i,j) and Cl(i, j) are the pixel values corresponding to the subset of l+1 and l. The formula was applied：

$$C^{l+1}(i,j)=\frac{C^{l}(i,j)}{\sum_{(m,n)\in S_l}K(i,j,m,n)}\sum_{(m,n)\in S_l}\frac{K(i,j,m,n)I(m,n)}{p^{l}(m,n)}$$

where $p^{l}(m,n)=\sum_{i,j}K(i,j,m,n)C^{l}(i,j)$, $(m,n)\in S_l$.

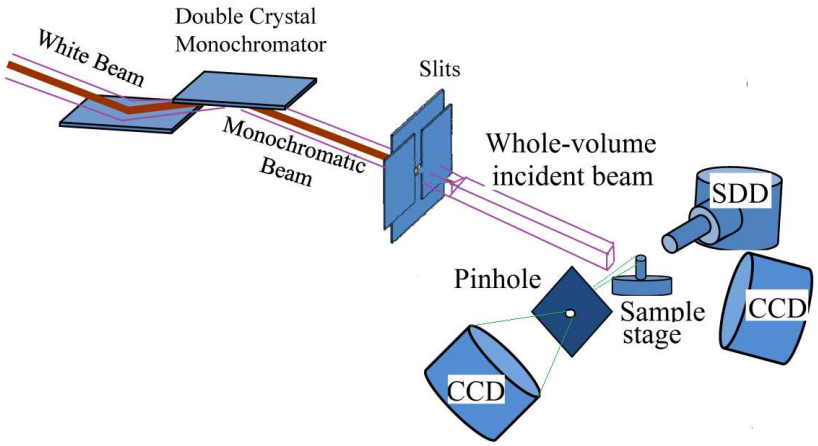

Fig.2 The layout of FF-XFCT at beamline BL13W1 of SSRF

Fig. 3(a) shows the FF-XFCT scheme and the cross section of 10-mm-diameter test sample which is made of polymethyl methacrylate (PMMA). Four holes with an diameter of 3 mm are distributed symmetrically, two nonadjacent holes are filled with cadmium(Cd) solution and another two holes are filled with iodine(I) solution. The equivalent concentrations of cadmium and Iodine are 100μg/ml.

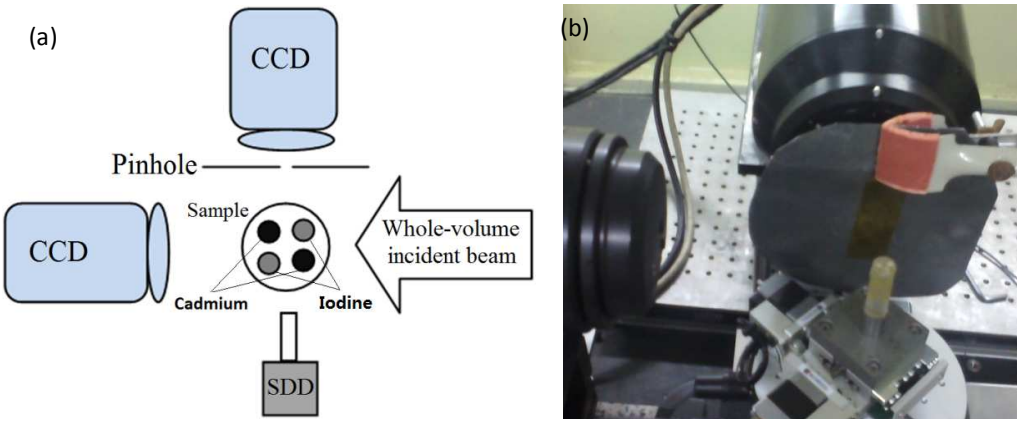

Fig. 3 The sketch of test sample and the photo of the prototype full filed XFCT

The FF-XFCT experiments were carried out at the beamline BL13W1 of SSRF. Fig.3(b) is the photo of FF-XFCT setup. A whole-volume incident beam of $15\times5mm^2$ was shaped by the X-ray slits. The photon flux rate in front of the object was approximately 2.0×10^{10} photons/mm^2/s. Tomography was performed at two different energies. Firstly, the incident energy is tuned to 33.5keV which is above the iodine K-edge of 33.17keV and above the cadmium K-edge of 26.71keV , and then tuned to 33.1keV which is below the iodine K-edge

and above the cadmium K-edge. A total of 180 projection images were collected for the test sample by rotating the sample from 0 to 180° in 1° steps. The X-ray fluorescence photons are collected by an X-ray CCD with pinhole collimator. The X-ray CCD camera is a cooled very high resolution X-ray sensitive CCD camera. The CCD sensor has resolution 4008 x 2670。The pixel size of the X-ray CCD is 72×72μm2（9μm×9μm with 8×8 binning） The first scintillator assembly is a short straight fibre-optic, on the front of which has been deposited a Gadolinium Oxysulphide X-ray scintillator. The input size of this scintillator is identical to the inherent input format of the camera, 36 x 24mm. The scintillator has been applied at a density of approx 5 mg/cm2。The camera features high-speed read-out of the CCD at 10 MHz, followed by digitisation of the CCD signal to 12-bit accuracy. This results in a maximum frame rate of approximately10 Hz with 8×8 binning. Exposure time for a single projection was 10s. Tomograms and the fluorescence spectrum were collected as pairs at 33.5keV and 33.1keV. Transmission CT have been acquired simultaneously by another X-ray CCD at 33.5keV and 33.1keV.

Results and Discussion

Fig.4 are the X-ray fluorescence spectrums and FF-XFCT sinograms obtained at two different energies. The FF-XFCT images were reconstructed by OSEM algorithm and transmission CT images were reconstructed by FBP algorithm[14]. The reconstruction time of OSEM for one slice is about one minutes when 6 subsets and 15 iterations were employed. Twenty slices were obtained by one FF-XFCT experiment. The reconstructed FF-XFCT slice of the phantom under double energies are show in fig.5(a-b). Fig.5(c) is acquired by separating FF-XFCT image at 33.5keV and 33.1keV.

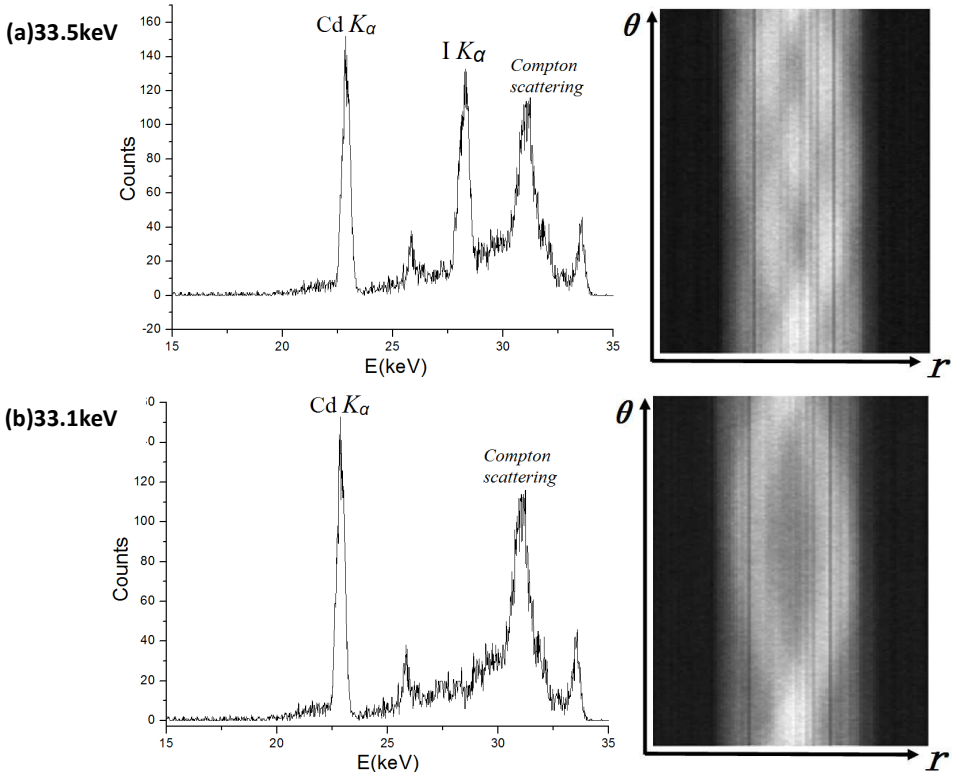

Fig. 4 The fluorescence spectrums and FF-XFCT sinograms obtained at two different energies. (a) 33.5keV; (b)33.1keV

There are Cd and I characteristic peaks at the fluorescence spectrums obtained at 33.5keV(Fig.4 (a)), it verify the presence of Cd and I in the illuminated area of the sample. We can get the Cd and I distributions by FF-XFCT(fig.5(a)), but we cannot identify which is Cd and which is I. There is only Cd characteristic peak at the fluorescence spectrums obtained at 33.1keV(Fig.4 (b)), so the image collected at 33.1keV is the cadmium distribution in the phantom(fig.5(b)). And then the imaging collected at 33.5keV was subtracted from the partnered imaging collected at 33.1keV resulting in the net iodine distribution and compartmentalization(fig.5(c)). A 3D cadmium and iodine distributions were built up by stacking the reconstructed slices together as shown in Fig. 6.

The transmission CT slices of the phantom under 33.5keV and 33.1keV (above/ below the iodine K-edge)are show in fig. 5(d-e). As expected, we maybe get the iodine image by K-edge subtracting imaging. Because of the low concentrations of iodine, we do not get the iodine image from the subtracting imaging in Fig.5(f). The results have shown that FF- XFCT is sensitive than conventional CT for low concentrations elements image. It's similar to the

results of Magdalena Bazalova's [15].

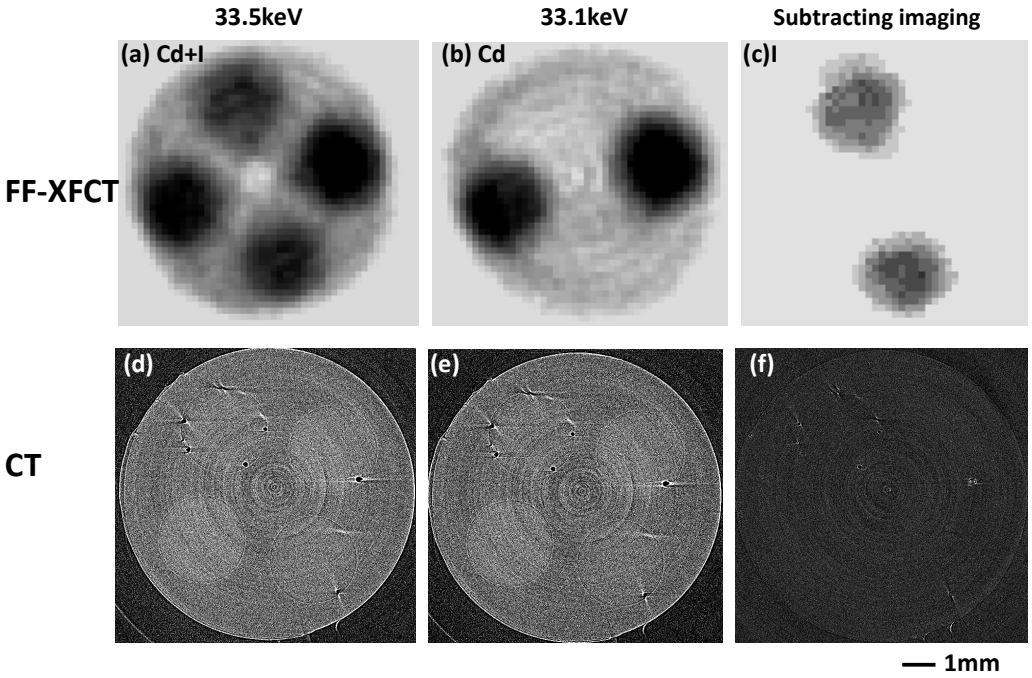

Fig.5 Reconstructed FF-XFCT and transmission CT slices of the phantom . (a) FF-XFCT slice at 33.5keV; (b) FF-XFCT slice at 33.1keV ;(c) FF-XFCT subtracting imaging;(d) CT slice at 33.5keV; (e)CT slice at 33.1keV;(f)CT subtracting imaging

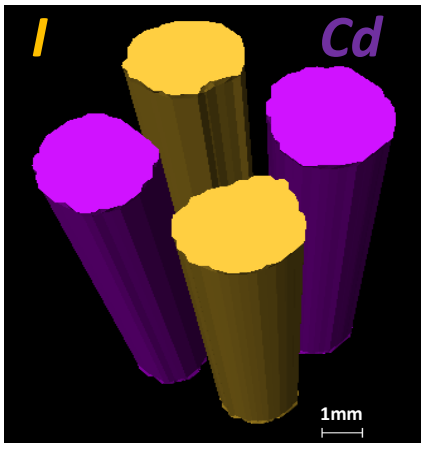

Fig.6 3D cadmium and iodine imaging obtained by FF-XFCT

In this paper, we present here a feasibility study to use synchrotron-based FF-XFCT with subtracting imaging to retrieve the 3D distribution of different elements. Energy tuning can be easily and precisely accomplished with the use of a monochromator at synchrotron beam lines over wide energy ranges. Using a FF-XFCT system with subtracting imaging, 3D elemental distributions for elements having absorption edges in the working energy range

can be retrieved. The results demonstrate FF-XFCT is a sensitive, inexpensive and simple approach for effective 3D element imaging.

Pinholes are an obvious first choice as image transfer optics for FF-XFCT, due to their simplicity, variable zoom possibility and low price. However, the transmission of a pinhole is rather low. The polycapillaries are likely to be efficient optics for FF-XFCT[16] . Future FF-XFCT will greatly benefit from advances in detector technology, as it will allow to use shorter exposure times, faster read-out and a higher quantum efficiency. Hong Liu. et al[16] have developed a novel approach for three-dimensional x-ray fluorescence mapping of gold nanoparticle-loaded objects in a physical phantom. We expect significant instrumental improvement in the years to come making 3D elemental sensitive imaging widely used.

ACKNOWLEDGEMENTS

The authors are grateful to colleagues at SSRF BL13W1 Beamline for their help on the experiments. This work was supported by National Natural Science Foundation of China grant no 11275257, U1232205,11375257,and by External Cooperation Program of Chinese Academy of Sciences grant no.GJHZ09058.

References

1. Bruno Golosio, Andrea Somogyi, Alexandre Simionovici, Pierre Bleuet, Jean Susini and Laurence Lemelle., *Applied Physics Letters*, 2004, 84:2199-2201
2. P. La Rivière, *Physics in Medicine and Biology*, 2004, 49:2391-2405
3. E. Miqueles and A. De Pierro, *IEEE TRANSACTIONS ON MEDICAL IMAGING*, 2010.30(2), 438 - 450
4. Tohoru Takeda, Jin Wu, Qingkai Huo, Tetsuya Yuasa, Kazuyuki Hyodo, F Avraham Dilmanian and Takao Akatsuka, *Journal of Synchrotron Radiation*, 2008,16: 57-62
5. Seong-Kyun Cheong, Bernard L Jones, Arsalan K Siddiqi, Fang Liu, Nivedh Manohar and Sang Hyun Cho. *Physics in Medicine and Biology,* 2010, 55: 647–662
6. Kuang Y, Pratx G, Bazalova M, Qian J, Meng B and Xing L. *Med. Phys*. 2013, 40(3),030701-1-7
7. Huo, Q., Sato, H., Yuasa, T., Akatsuka, T.,Wu, J., Lwin, T., Takeda, T.& Hyodo, K. *X-ray Spectrom*. 2009,38, 439–445.
8. Geng Fua and Ling-Jian Meng , *Med. Phys.* 2013, 40(6), 061903-1-11
9. O. Scharf, S. Ihle, I. Ordavo, V. Arkadiev, A. Bjeoumikhov, S. Bjeoumikhova, G. Buzanich, R. Gubzhokov, A. G∈unther, R. Hartmann, M. K∈uhbacher, M. Lang, N. Langhoff, A. Liebel, M. Radtke, U. Reinholz, H. Riesemeier, H. Soltau, L. Struder, A. F. Thunemann, and R. Wedell, *Anal Chem*, 2011, 83, 2532-2538.

10. Ordavo, I.; Ihle, S.; Arkadiev, V.; Scharf, O.; Soltau, H.; Bjeoumikhov, A.; Bjeoumikhova, S.; Buzanich, G.; Gubzhokov, R.; Günther, A.; Hartmann, R.; Holl, P.; Kimmel, N.; Kühbacher, M.; Lang, M.; Langhoff, N.; Liebel, A.; Radtke, M.; Reinholz, U.; Riesemeier, H.; Schaller, G.; Schopper, F.; Strüder, L.; Thamm, C.; Wedell, R., *Nucl. Instrum. Meth. A* ,2011,654(1) 250-257
11. Naoki Sunaguchia, Tetsuya Yuasab, Kazuyuki Hyodoc and Tsutomu Zeniyad, *Optics Communications*,2013, 297, 210–214
12. Freek Beekman, Frans van der Have, *European Journal of Nuclear Medicine and Molecular Imaging* , 2007, 34:151-161
13. Qun Yang, Biao Deng, Weiwei Lv, Fei Shen, Rongchang Chen, Yudan Wang, Guohao Du, Fuhua Yan, Tiqiao Xiao and Hongjie Xu, *J. Synchrotron Rad*. 2012. 19, 210–215
14. R. C. Chen, D. Dreossi, L. Mancini, R. Menk, L. Rigon, T. Q. Xiao, and R. Longo, *Journal Of Synchrotron Radiation* , 2012,19, 836-845
15. Magdalena Bazalova, Yu Kuang, Guillem Pratx, and Lei Xing. *IEEE TRANSACTIONS ON MEDICAL IMAGING*,2012, 31(8), 1620-1627
16. M. Alfeld, K. Janssens, A. Sasov, X. Liu, A. Kostenko, K. RickersAppel, and G. Falkenberg, *AIP Conference Proceedings*,2010, 1221, 111-118
17. Liqiang Ren, Di Wu, Yuhua Li, Ge Wang, Xizeng Wu, and Hong Liu, *Medical Physics*,2014, 41(3), 031902-1-12